**Atmospheric
Chemistry
and Physics**

Growth in NO$_x$ emissions from power plants in China: bottom-up estimates and satellite observations

S. W. Wang[1], Q. Zhang[2], D. G. Streets[3], K. B. He[1], R. V. Martin[4,5], L. N. Lamsal[6,7], D. Chen[8], Y. Lei[9], and Z. Lu[3]

[1]State Key Joint Laboratory of Environment Simulation and Pollution Control, School of Environment, Tsinghua University, Beijing, China
[2]Ministry of Education Key Laboratory for Earth System Modeling, Center for Earth System Science, Tsinghua University, Beijing, China
[3]Decision and Information Sciences Division, Argonne National Laboratory, Argonne, IL, USA
[4]Department of Physics and Atmospheric Science, Dalhousie University, Halifax, NS, Canada
[5]Harvard-Smithsonian Center for Astrophysics, Cambridge, MA, USA
[6]Goddard Earth Sciences Technology and Research, Universities Space Research Association, Columbia, MD, USA
[7]NASA Goddard Space Flight Center, Greenbelt, MD, USA
[8]Department of Atmospheric and Oceanic Sciences, University of California at Los Angeles, Los Angeles, CA, USA
[9]Key Laboratory of Environmental Planning and Policy Simulation, Chinese Academy for Environmental Planning, Beijing, China

Correspondence to: Q. Zhang (qiangzhang@tsinghua.edu.cn)

Abstract. Using OMI (Ozone Monitoring Instrument) tropospheric NO$_2$ columns and a nested-grid 3-D global chemical transport model (GEOS-Chem), we investigated the growth in NO$_x$ emissions from coal-fired power plants and their contributions to the growth in NO$_2$ columns in 2005–2007 in China. We first developed a unit-based power plant NO$_x$ emission inventory for 2005–2007 to support this investigation. The total capacities of coal-fired power generation have increased by 48.8 % in 2005–2007, with 92.2 % of the total capacity additions coming from generator units with size $\geq$300 MW. The annual NO$_x$ emissions from coal-fired power plants were estimated to be 8.11 Tg NO$_2$ for 2005 and 9.58 Tg NO$_2$ for 2007, respectively. The modeled summer average tropospheric NO$_2$ columns were highly correlated ($R^2 = 0.79$–0.82) with OMI measurements over grids dominated by power plant emissions, with only 7–14 % low bias, lending support to the high accuracy of the unit-based power plant NO$_x$ emission inventory. The ratios of OMI-derived annual and summer average tropospheric NO$_2$ columns between 2007 and 2005 indicated that most of the grids with significant NO$_2$ increases were related to power plant construction activities. OMI had the capability to trace

the changes of NO$_x$ emissions from individual large power plants in cases where there is less interference from other NO$_x$ sources. Scenario runs from GEOS-Chem model suggested that the new power plants contributed 18.5 % and 10 % to the annual average NO$_2$ columns in 2007 in Inner Mongolia and North China, respectively. The massive new power plant NO$_x$ emissions significantly changed the local NO$_2$ profiles, especially in less polluted areas. A sensitivity study found that changes of NO$_2$ shape factors due to including new power plant emissions increased the summer average OMI tropospheric NO$_2$ columns by 3.8–17.2 % for six selected locations, indicating that the updated emission information could help to improve the satellite retrievals.

1 Introduction

Nitrogen oxides (NO$_x \equiv$ NO + NO$_2$) play an important role in the photochemical production of tropospheric ozone and are detrimental to human health and the ecosystem. NO$_x$ is released to the troposphere as a result of anthropogenic (e.g., fossil-fuel and biofuel combustion and human-induced

biomass burning) and natural (e.g., soil emissions, wildfires and lightning) phenomena. During the past two decades, anthropogenic NO_x emissions from China have surged simultaneously with the rapid growth in China's economy and hence attract the attention of scientists and policy makers. Coal-fired power plants are the largest coal consumer in China and are believed to be the largest contributor to China's NO_x emissions (Hao et al., 2002; Zhang et al., 2007). Since 2005, hundreds of large electricity generator units have been constructed all over China. As a result, the total capacity of coal-fired power plants has increased by 49 %, from 328 GW in 2005 to 489 GW in 2007.

An understanding of the growth of power plant NO_x emissions in China and subsequently a reliable evaluation of their environmental effects using atmospheric chemical models largely depends on how accurately we know the emission budget. NO_x emission inventories are traditionally developed by integrating the emissions from all known source types using the fuel consumption data and emissions factors (e.g., Streets et al., 2003), which is the so-called bottom-up approach. China's coal-fired power plant NO_x emissions have been estimated in many studies (Hao et al., 2002; Streets et al., 2003; Tian, 2003; Ohara et al., 2007; Zhang et al., 2007, 2009a; Zhao et al., 2008). However, the inaccurate information of the locations of power plants (except for Zhao et al., 2008), due to limited access to specific information about point sources in China, is always a defect for studies on individual power plant emissions and seems to lead to intrinsic regional discrepancies between modeled NO_2 columns and satellite measurements over China (e.g., Zhao and Wang, 2009; Lin et al., 2010). Although the uncertainties in power plant emissions are believed to be far less than for other sources (Zhang et al., 2009a), reliable validation of the power plant NO_x emissions with independent measurements is still a gap in China.

Remote sensing instruments provide valuable continuous observation data for tracing and evaluating NO_x emissions from surface sources. During the past two decades, polar-orbiting satellite instruments such as the Global Ozone Monitoring Experiment (GOME), SCanning Imaging Absorption SpectroMeter for Atmospheric CHartographY (SCIAMACHY), Ozone Monitoring Instrument (OMI), and GOME-2, have sent back spatio-temporally continuous observations of the trace gases and aerosols in the atmosphere. These measurements greatly extended our insights into the temporal trends of atmospheric NO_2 concentrations (e.g., Richter et al., 2005; van der A et al., 2008) and their atmospheric transport (e.g., Wenig et al., 2003), and were applied to derive "top-down" constraints on surface NO_x emissions (Martin et al., 2003, 2006; Jaeglé et al., 2005; Konovalov et al., 2006; Wang et al., 2007; Lin et al., 2010, 2012; Lamsal et al., 2011) with the aid of chemical transport models.

With the improvement of the spatio-temporal resolution of satellite instruments, especially OMI, they have been proved to be capable in monitoring emissions from large point sources. Kim et al. (2006, 2009) found excellent correlations between the satellite measurements (SCIAMACHY and OMI) and WRF-Chem simulations over grids dominated by large power plants in the western United States, benefiting from the Continuous Emission Monitoring System (CEMS) data used in their studies. Carn et al. (2007) observed dense SO_2 concentrations around the copper smelters in Peru using OMI and estimated their SO_2 emissions. Ghude et al. (2008) identified major NO_x emission hot spots in India using GOME and SCIAMACHY and analyzed the emission trends and seasonal cycle. In our previous work, we found that the dramatic changes of OMI-derived summertime NO_2 and SO_2 columns in Inner Mongolia, China, could be attributed to power plant construction activities and operation of flue-gas desulfurization (FGD) devices (Zhang et al., 2009b; Li et al., 2010), and the growth rates of NO_x emissions in the regions where new power plants were constructed could be even quantified by OMI observations (Wang et al., 2010). Lin and McElroy (2011) used thermal power generation (TPG) as the proxy of economy and found that the changes in OMI NO_2 columns were consistent with changes in TPG. They further concluded that OMI NO_2 observations were capable of detecting the variations in NO_x emissions stimulated by economy change. However, the contribution of power plants to the overall emission changes was not separated in their work.

In this work, we aim to portray an overall view of the changes of power plant NO_x emissions in China during 2005–2007 based on bottom-up emission inventory and satellite observations, and evaluate their contributions to the growth of NO_2 concentrations in China. Section 2 presents the methodology of the unit-based power plant emission inventory and the chemical transport model, as well as the OMI retrievals used in this study. We present the power plant NO_x emissions in China in 2005–2007 in Sect. 3 and validate their accuracy using OMI measurements in Sect. 4. Section 5 portrays the growth of power plant NO_x emissions viewed by OMI and quantifies their contributions to the growth of regional NO_2 columns with GEOS-Chem. The impacts of the newly added power plant emissions on the a priori NO_2 profiles used in the satellite retrievals are discussed in Sect. 6. Section 7 summarizes the conclusions of this study.

2 Methodology

2.1 Unit-based power plant emission inventory

We develop a unit-based power plant NO_x emission inventory for the time period of 2005–2007 for mainland China. Detailed information of ∼5700 generator units was collected for this work, including geographical location, boiler size, coal consumption per unit electricity supply, emission

control technology, and the exact month in which the unit formally came into operation and closed.

Monthly NO_x emissions are calculated by each unit according to the technology and operation information, following the equation of Wang et al. (2010):

$$E_i = \sum_j \sum_k \sum_m 1.4 \times U_{i,j} \times T_{i,j} \times F_i \times C_{i,j} \times EF_{k,m} \times 10^{-6}$$

(1)

where i, j, k, m stand for province, generator unit, boiler size, and emission control technology; 1.4 is the mass scaling factor from standard coal to raw coal; E is the monthly NO_x emissions (Mg); U is the unit size (MW); T is the annual operation hours; F is the monthly fraction of annual total electricity generation; C is the specific coal consumption per unit electricity supply (gram coal equivalent kWh^{-1}); and EF is the emission factor ($g\,kg^{-1}$). The dynamical NO_x emission factors adopted from Zhang et al. (2007) vary between 5.6 and 10.5 $g\,kg^{-1}$ coal burned based on boiler size and the presence or absence of low-NO_x-burner (LNB), which are comparable to the values of 4.0–11.5 $g\,kg^{-1}$ used in Zhao et al. (2008).

2.2 GEOS-Chem Model

We simulate tropospheric NO_2 columns over China for the years 2005–2007 using the nested-grid GEOS-Chem model. The GEOS-Chem model is a global 3-D chemical transport model (CTM) for atmospheric composition including a detailed simulation of tropospheric ozone-NO_x-hydrocarbon chemistry as well as of aerosols and their precursors (Bey et al., 2001). The chemical mechanism includes >80 species and >300 reactions. The GEOS-Chem model is driven by assimilated meteorological fields from the Goddard Earth Observing System (GEOS) at the NASA Global Modeling and Assimilation Office (GMAO: http://gmao.gsfc.nasa.gov/). In this paper we use the nested-grid GEOS-Chem model (v8-02-01) developed by Chen et al. (2009) with GEOS-5 at native horizontal resolution of $0.5° \times 0.667°$. The nested-grid GEOS-Chem model is embedded into the coarse-resolution global model ($4° \times 5°$) through the one-way nested approach, propagating the time-varying boundary conditions from the global model with consistent meteorology, dynamics, and chemistry. The nested domain stretches from $11°$ S to $55°$ N and from $70°$ E to $150°$ E, covering most of East/Southeast Asia. GEOS-5 meteorological data are provided every 3–6 h (3 h for surface fields and mixing depths) for 72 hybrid pressure sigma levels in the vertical extending up to 0.01 hPa. For computational expedience the vertical levels above the lower stratosphere are merged, retaining a total of 47 vertical levels, with 14 pure sigma levels resolved within 2 km altitude. In this work, we conduct 3-yr full-chemistry simulations for 2005–2007.

The global anthropogenic emissions are from EDGAR (Olivier and Berdowski, 2001) for the base year of 2000 and scaled to 2006 following van Donkelaar et al. (2008). We then replaced the anthropogenic NO_x emission inventory over China with our own estimates. For power plant emissions we use the unit-based inventory for 2005–2007 described in Sect. 2.1. Other anthropogenic NO_x emissions and monthly variations were developed for the years 2005–2007 following the methodology described in Zhang et al. (2007), with dynamic emission factors to reflect the technology innovations. Emissions for other parts of East/Southeast Asia are replaced by the INTEX-B inventory for 2006 (Zhang et al., 2009a). The GEOS-Chem model also includes NO_x emissions from soils (Yienger and Levy, 1995; Wang et al., 1998), lightning (Sauvage et al., 2007), biomass burning (van der Werf et al., 2006), biofuel (Yevich and Logan, 2003), aircraft (Baughcum et al., 1996), and stratospheric flux. Table 1 summarizes the NO_x emissions over China used in this work.

A 1-yr spin-up was conducted to remove the effects of the initial concentration fields. Monthly varying tropopause heights were used to derive the tropospheric NO_2 columns. Daily 2-h early afternoon modeled tropospheric NO_2 columns were averaged at the local time of 13:00–15:00 h. To be consistent with the OMI observations, we sampled the model at grids coincident with the daily satellite pixels used in the final average columns.

2.3 OMI tropospheric NO_2 column densities

The OMI aboard the Aura satellite is a nadir-viewing imaging spectrograph measuring the earthshine radiance and the solar irradiance in the ultraviolet-visible range from 264 to 504 nm (Levelt et al., 2006). The Aura spacecraft, the last of the EOS observatories, was launched on 15 July 2004, into a sun-synchronous polar orbit at 705 km altitude with a $98.2°$ inclination and a local equator-crossing time of 13:45 h in ascending node. OMI measures the complete spectrum with the nadir pixel size of 24×13 km^2 and daily global coverage.

The NO_2 abundance is quantified along the viewing path (slant column) using DOAS (Differential Optical Absorption Spectroscopy) (Platt, 1994; Boersma et al., 2002; Bucsela et al., 2006) for each pixel. The air mass factor (AMF), defined as the ratio of the slant column abundance to the vertical column abundance, can be formulated as the integral of the relative vertical distribution (shape factors), weighted by altitude-dependent coefficients (scattering weight factors) for optically thin atmospheric species (Palmer et al., 2001).

In this work, the tropospheric slant NO_2 column densities are from the DOMINO product (version 1.0.2, collection 3) (Boersma et al., 2007) available from the Tropospheric Emission Monitoring Internet Service (TEMIS) (http://www.temis.nl/). The tropospheric slant column density is obtained by removing the stratospheric contribution estimated from assimilating slant columns provided by a global CTM, the TM4 model (Dirksen et al., 2011). The

Source	Annual Emissions (Tg NO_2)		
	2005	2006	2007
Power plants	8.11	8.92	9.58
Other anthropogenic sources*	10.69	11.78	13.77
Biomass burning	0.15	0.20	0.23
Soils and fertilizers	1.71	1.75	1.77
Lightning	0.83	0.90	0.59
Aircraft	0.05	0.05	0.05

*Including industry, transportation, and biofuel NO_x emissions.

cross-track biases were then determined using the average NO_2 slant column densities in the 5th to 95th percentile limits over less polluted areas (30° S–5° N) and removed from the tropospheric slant column densities for each orbit dataset, following the approach described by Celarier et al. (2008) and Lamsal et al. (2010). Correction of the cross-track bias is estimated to cause ∼5 % decrease in the average tropospheric NO_2 column (Lamsal et al., 2010).

The tropospheric vertical NO_2 column retrieval is sensitive to the a priori NO_2 shape factors. Lamsal et al. (2010) developed an alternative OMI product (DP_GC) based on the DOMINO product and validated its accuracy in summer using in-situ measurements carried out in the United States. They used NO_2 shape factors generated from GEOS-Chem (2° × 2.5° with GEOS-4 meteorology fields) in DP_GC and Average Kernels (A_k) from the DOMINO product to reproduce the AMF for each OMI pixel in order to improve the representation in NO_2 shape factors generated by TM4, which have been found to be insufficiently mixed throughout the boundary layer due to the inconsistency in model sampling (Hains et al., 2010; Boersma et al., 2011) and to ensure self-consistency when compared the OMI retrievals with GEOS-Chem modeled columns (Eskes and Boersma, 2003; Boersma et al., 2004).

In this work, we follow the method in Lamsal et al. (2010) but use NO_2 shape factors provided by the nested-grid GEOS-Chem simulation described in Sect. 2.2 to calculate the local AMF. The high-resolution shape factors (0.5° × 0.666°) simulated with year-by-year emission inputs improve the representation of the real vertical distributions in OMI pixels and also consider changes in the NO_2 shape factors related to the changes of NO_x emissions. The effects of newly added power plant emissions on NO_2 shape factors and OMI retrievals will be discussed in Sect. 6.

We used only OMI pixels with solar zenith angle ≤70° and cloud radiance fraction ≤0.3 in the final average columns. Pixels at swath edges (five pixels on each side) were rejected to reduce spatial averaging. Since 25 June 2007 the cross-track positions 53–54 (0-based) in

the OMI data are specified as a row anomaly due to the effect of a partial external blockage of the radiance port on the instrument (http://www.knmi.nl/omi/research/product/rowanomaly-background.php). These affected pixels were removed. Finally, each OMI pixel was allocated by area-weights into 0.5° × 0.667° grids with corner coordinate information to achieve daily global tropospheric vertical NO_2 column maps.

3 Power plant NO_x emissions in China, 2005–2007

3.1 New power plants

We refer to the power plants with generator units coming into operation in 2005–2007 hereinafter as "new power plants" in this paper. The total capacities of coal-fired power generation have increased by 48.8 %, from 328.4 GW at the beginning of 2005 to 488.8 GW at the end of 2007. The new generator units are mainly concentrated in five provinces (see Table 2), which are Inner Mongolia (18.6 GW), Jiangsu (17.3 GW), Zhejiang (12.5 GW), Shandong (12.2 GW), and Henan (11.2 GW), accounting for 45.0 % of the total capacity additions.

Why have new power plants surged in just two years? Rapid development of the economy and high energy-consuming industry contributed to a shortage of electricity generation in the first few years of this century in China. As a result, as many as 22 provinces in China limited their electricity supply to some extent in 2003. In this context, a batch of large generator units was immediately licensed for construction and consequently came into operation during 2005–2007.

Most of the new generator units are large. Figure 1 shows the changes of total capacities for different sizes of generator units in 2004–2007. The capacities of generator units with size <300 MW are 171.3 GW in 2004, and remain almost constant in magnitude for the following three years. In contrast, 92.2 % of the total capacity additions in 2005–2007 are from generator units with size ≥300 MW. This reflects the huge electricity demand and also corresponds to a structural readjustment in the power sector aimed at energy conservation and emission reduction. It is noteworthy that generator units with size ≥600 MW began to come into operation throughout the country since 2006, with total capacity increasing from 38.8 GW at the beginning of 2005 to 132.4 GW at the end of 2007, a factor of 3.4. As a result, the proportion of generator units with size <300 MW decreased from 52.2 % in 2004 to 37.6 % at the end of 2007.

3.2 Power plant NO_x emissions

As a consequence of the new power plant construction, annual power plant NO_x emissions increased from 8.11 Tg in 2005 to 9.58 Tg in 2007 in China, based on our unit-based power plant NO_x emission inventory. Figure 2 shows

Table 2. Annual and summer (June to August) NO$_x$ emissions from coal-fired power plants in 2005–2007 in mainland China.

| Region | NO$_x$ Emissions (Gg NO$_2$ a^{-1}) | | | | | | New Capacities* |
| | 2005 | | 2006 | | 2007 | | |
	Annual	Summer	Annual	Summer	Annual	Summer	(MW)
Anhui	222.3	61.8	243.8	70.7	270.4	76.0	6860
Beijing	82.4	22.0	73.9	17.9	75.6	20.1	0
Chongqing	79.2	17.3	100.7	25.3	117.3	24.6	2700
Fujian	144.7	32.1	157.8	34.2	199.6	52.1	4800
Gansu	123.0	28.9	124.0	27.1	144.2	30.8	2150
Guangdong	467.6	114.1	510.5	123.0	561.7	155.8	8910
Guangxi	110.2	22.9	114.5	22.0	125.9	24.5	1800
Guizhou	245.0	63.7	292.8	73.3	302.6	71.0	5500
Hainan	17.7	5.1	19.0	5.5	24.2	7.2	660
Hebei	517.3	137.8	519.6	139.1	559.6	142.5	6730
Heilongjiang	300.8	68.4	332.6	77.0	325.4	80.5	3115
Henan	637.3	168.2	650.4	171.2	725.2	180.3	11 210
Hubei	209.3	53.9	243.1	63.9	257.2	60.9	2600
Hunan	127.6	33.8	174.5	45.0	183.5	40.9	5450
Inner Mongolia	452.6	100.6	584.3	138.3	684.2	167.6	18 574
Jiangsu	748.8	205.3	800.2	217.0	817.0	221.5	17 335
Jiangxi	137.2	35.0	139.6	35.1	148.8	40.7	3330
Jilin	209.3	46.4	229.3	56.7	234.3	59.0	2260
Liaoning	389.2	92.4	424.8	108.9	438.1	109.2	4270
Ningxia	110.9	26.2	132.4	37.2	147.5	34.0	3180
Qinghai	26.4	6.3	32.3	7.7	36.0	8.3	0
Shaanxi	191.9	41.5	208.2	53.2	235.5	57.1	4530
Shandong	861.3	226.3	925.4	242.5	974.8	258.7	12 240
Shanghai	187.9	50.1	181.1	50.1	180.7	48.1	0
Shanxi	496.0	130.3	540.0	136.1	567.6	143.2	9500
Sichuan	248.8	60.0	267.3	71.3	252.4	51.0	4290
Tianjin	116.6	31.2	114.1	29.0	120.3	34.8	600
Tibet	0	0	0	0	0	0	0
Xinjiang	126.7	34.7	142.7	37.9	157.6	42.3	890
Yunnan	147.4	32.0	194.9	43.7	205.3	45.9	5400
Zhejiang	370.6	96.0	442.2	111.6	503.6	140.5	12 505
China Total	8105.6	2044.6	8916.1	2271.6	9576.3	2429.1	161 389

*Capacities of new generator units which came into operation in 2005–2007.

the spatial distributions of annual power plant NO$_x$ emissions for 2005 and 2007 and the changes. The changes shown in Fig. 2c clearly illustrate the locations of the new power plants and magnitudes of their NO$_x$ emissions. Table 2 summarizes the annual and summer (June–August) power plant NO$_x$ emissions by province for 2005–2007 in mainland China. The growth rate of NO$_x$ emissions between 2005 and 2007 in the power sector (18.1 %) is less than the growth rates of total capacity (48.8 %) and coal consumption (26.5 %) in coal-fired power plants, reflecting improvements in energy efficiency and emission control technology in new generator units and reduced annual operating hours. The ≥600 MW generator units contribute 27.1 % to capacity, consume 20.7 % of the coal, and release 16.0 % of the power plant NO$_x$ to the atmosphere in 2007. In contrast, the

≤100 MW generator units contribute 16.8 % to capacity, but consume 23.2 % of the coal, and emit 32.8 % of the power plant NO$_x$ in 2007. Though emissions generally increase throughout the country, as revealed by Fig. 2, Beijing and Shanghai show downward trends because of the migration of coal-fired power plants away from these two metropolitan areas.

The 2006 annual emissions are within 3 % of the 9.20 Tg estimate in the INTEX-B emissions inventory (Zhang et al., 2009a), because of the similar province activity data and emission factors used in these two inventories. Our annual power plant NO$_x$ emission estimates for 2005 are 16 % higher than the value of 6.97 Tg in another unit-based power plant inventory (Zhao et al., 2008). This difference could be
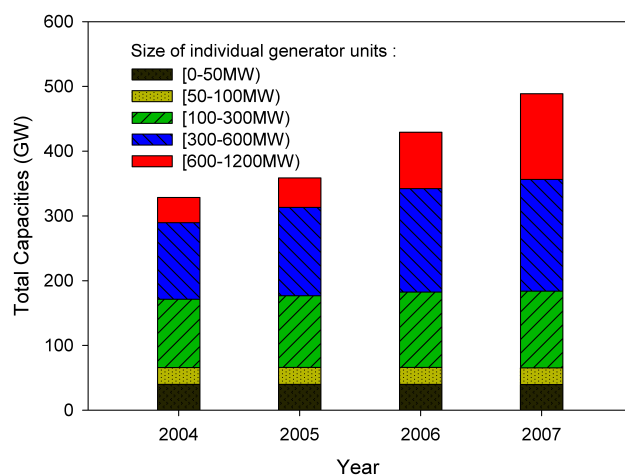
Fig. 1. Changes of total capacities for different sizes of coal-fired generator units in 2004–2007 in China.

Table 3. Reduced Major Axis regression analysis between OMI (x-axis) and GEOS-Chem (y-axis) summer (June to August) average NO$_2$ columns in 2005 and 2007.

Date	Regression	Case A	Case B	Case C
	Slope	0.86	0.74	0.75
	Offset	0.06	0.06	−0.03
2005-JJA	R^2	0.82	0.78	0.85
	Samples*	106	615	2968
	Slope	0.93	0.89	0.83
	Offset	−0.25	−0.35	−0.13
2007-JJA	R^2	0.79	0.62	0.74
	Samples*	125	556	2851

*Only grids with OMI sample number ≥10 are used.

attributed to the use of different emission factors in the two inventories.

Using a Monte-Carlo approach described in Zhao et al. (2011), the average uncertainty of this inventory is estimated to be −20 % to 19 % (at 95 % coincident intervals). Also the uncertainties related to geographical location have been significantly reduced in our unit-based power plant emission inventory compared to previous "bottom-up" estimates. However, uncertainty for an individual unit could be larger because unified emission factors and annual operation hours were applied to group of units. In the US, NO$_x$ emission rates for most power plants are measured by CEMS, which represent one of the most accurate parts of the US emission database, but this is not the case for China. Average emission factors from limited local measurements were used for all generator units with similar technologies, which ignored possible variations among individual units and will introduce some uncertainties. Also, the monthly profile was calculated for each province using the monthly fraction of annual total electricity generation and applied to all generator units in the province. This algorithm will not affect the total NO$_x$ emission budget but downgrade the accuracy for individual plant estimates, as it misses the variations of operating conditions among individual generator units. We estimate a typical uncertainty level of −42 % to 51 % for an individual unit by using Monte-Carlo approach.

4   Evaluation of power plant NO$_x$ inventory by OMI observations

Power plants in China are often located in populated areas where there is a mix of various anthropogenic NO$_x$ sources, such as industrial complexes and vehicles, which adds difficulties to the validation of power plant emissions. To further investigate the impact of the uncertainties associated with

other anthropogenic emissions on the evaluation of the power plant inventory, we compare the modeled and observed NO$_2$ columns over three categories of grids in China as the following three cases: grids dominated by power plant NO$_x$ emissions (Case A), all grids with power plants (Case B), and all grids in China (Case C). Case A is defined as grids with urban population <0.5 million and power plant NO$_x$ emissions >60 % of total NO$_x$ emissions. The urban population data are obtained by masking the LandScan 2006 1 km × 1 km resolution population density (Bhaduri et al., 2002) using Moderate Resolution Imaging Spectroradiometer (MODIS) urban land use fraction data (Schneider et al., 2009) and then degraded to 0.5° × 0.667° resolution. Grids with urban population <0.5 million are generally associated with rural areas or small towns in China.

The modeled summer average tropospheric NO$_2$ columns are compared with OMI measurements for the three cases in Figs. 3–5 and Table 3. We only used summer data for comparison, as NO$_2$ columns have a closer relationship to local emissions in summer than other seasons due to the shorter lifetime of NO$_x$ in summer. However, South China and the Sichuan Basin are frequently covered by cloud in summer, resulting in insufficient observation samples in these regions (see Fig. 7). We use only grids with OMI sample number ≥10 to conduct the validation in those regions.

Figure 3 presents the relationship between model and OMI NO$_2$ columns over the grids where power plant emissions are dominant (Case A) for 2005 and 2007. The grids are colored by the regions defined in Fig. 2. Only ∼4 % of total samples over China were left (see Table 3) after using the filtering criterion described above. As presented in Table 3, modeled columns are 7–14 % lower than OMI retrievals, within the uncertainty range of the power plant emission estimates. The spatial correlations are high ($R^2 = 0.79$–0.82) with little scatter, lending support to the high accuracy of the unit-based power plant NO$_x$ emission inventory. Also it should be noted that emissions in the power plant dominant grids are represented by total NO$_x$ emissions, including other
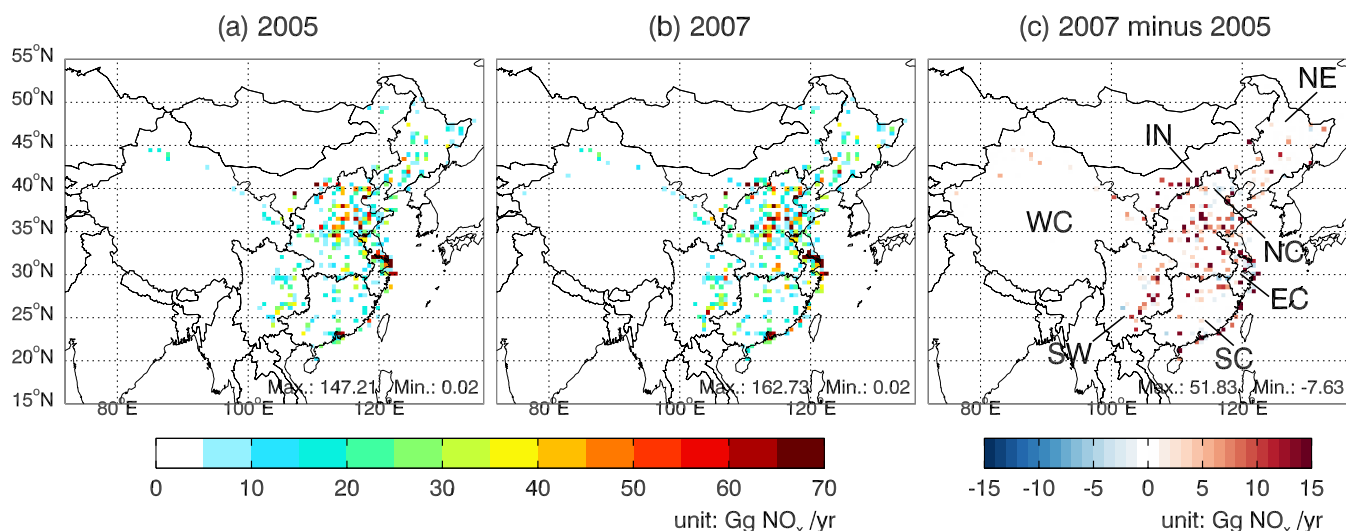
Fig. 2. Spatial distributions of annual coal-fired power plant NO$_x$ emissions for 2005 and 2007 and the changes. The maximum values and minimum values are indicated. Solid lines within the Chinese national boundaries denote the seven regions discussed in the text: NE-Northeast China, IN-Inner Mongolia, NC-North China, EC-East China, SC-South China, SW-Southwest China, and WC-West China.
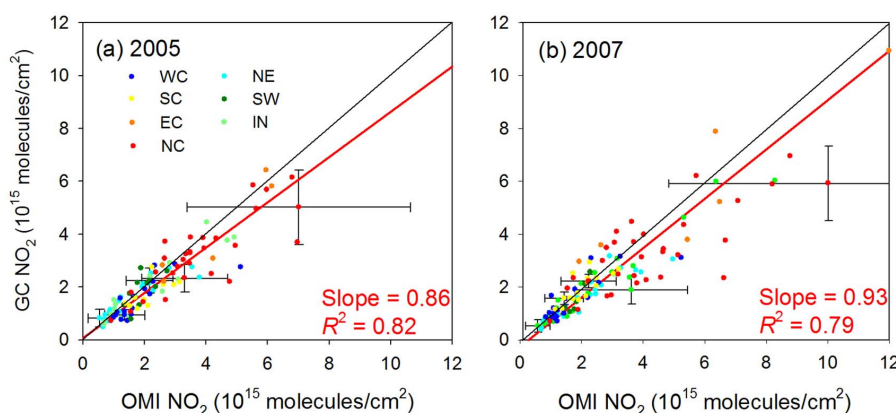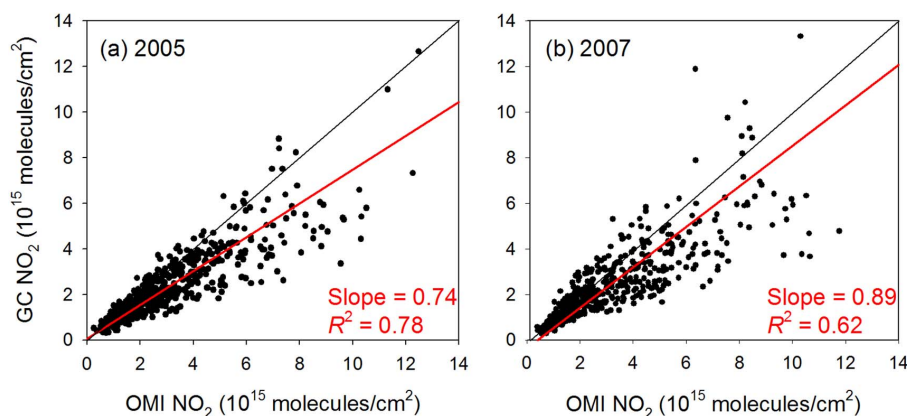

Fig. 3. Comparisons between GEOS-Chem and OMI summer average tropospheric NO$_2$ columns for **(a)** 2005 and **(b)** 2007 over power plant dominant grids in China. Grids are colored by the regions defined in Fig. 2. The linear fit regression (red line) is based on Reduced Major Axis (RMA) algorithm (Clarke, 1980). Error bars indicate the standard deviations in the summer average columns (only shown for minimum, quartiles, and maximum points in OMI datasets).

anthropogenic emissions, and remotely sensed urban extent, which may or may not be accurate. In previous work it has been concluded that anthropogenic NO$_x$ emission estimates for industry and transportation can be significantly underestimated for a specific grid (Zhang et al., 2007; Wang et al., 2010). This probably causes the significant low bias of the modeled NO$_2$ columns for several grids in North China (see Fig. 3b), where emissions from industries and vehicles are high. Using a threshold in which power plant NO$_x$ emissions exceed 80 % of total NO$_x$ emissions (instead of 60 %) further improves the R^2 to 0.77–0.91 and slopes to 0.89–0.97, but with only <1 % samples remaining.

Excellent correlations between WRF-Chem modeled and satellite based NO$_2$ columns over power plant plumes were also observed in western United States regions dominated by power plant NO$_x$ emissions (Kim et al., 2006, 2009). Those good agreements were partly benefited from the highly accurate NO$_x$ emission data measured by CEMS. In this work, although our unit-based power plant NO$_x$ emission estimates for individual generator units would not have accuracy as high as CEMS measurements, the similar excellent agreements between model and OMI NO$_2$ columns (slope = 0.86–0.93, $R = 0.89$–0.90) may support reasonably high accuracy of our emission estimates. Considering the uncertainties in bottom-up inventories (Zhao et al., 2011), satellite retrievals (Boersma et al., 2004), and the coarse resolution of GEOS-Chem compared to the original fine footprint of OMI, we can

Fig. 4. Comparisons between GEOS-Chem and OMI summer average tropospheric NO$_2$ columns for **(a)** 2005 and **(b)** 2007 over grids with power plants in China. RMA algorithm is used in the linear fitting (red line).
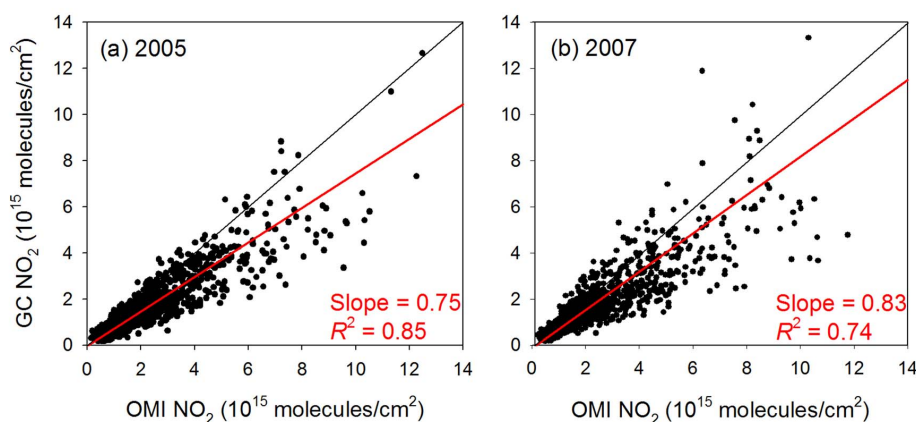
Fig. 5. Comparisons between GEOS-Chem and OMI summer average tropospheric NO$_2$ columns for **(a)** 2005 and **(b)** 2007 over all grids in China. RMA algorithm is used in the linear fitting (red line).

conclude that the unit-based power plant NO$_x$ emissions developed in this work are reasonably reliable.

We next plotted the correlations between modeled and OMI observed NO$_2$ columns for all grids with power plant NO$_x$ emissions (Case B) in Fig. 4, which include ∼20 % of the total samples over China (see Table 3). Compared with Case A, the R^2 values decreased to 0.62–0.78 with considerable scatter observed in grids with elevated NO$_2$ concentrations, indicating that total NO$_x$ emissions are relatively poorly understood over regions where power plant emissions are mixed with other anthropogenic sources. Other anthropogenic emission inventories used in this work are thought to be much more uncertain than the unit-based power plant inventory, as they were estimated at provincial level and then allocated to each grid using various spatial proxies such as population density and road networks (Streets et al., 2003). The uncertainties induced by this "top-down" assignment method could be large for a specific grid, which may result in relatively poor model performance over many grids. However, assessing the uncertainties introduced by the emission

gridding process is beyond the scope of this paper and will need to be investigated in future work.

Tropospheric NO$_2$ columns over all grids in China (Case C) also have good spatial correlations between model and OMI with R^2 of 0.85 and 0.74 for 2005 and 2007 respectively, as shown in Fig. 5. Modeled NO$_2$ columns are 17–25 % lower than OMI, with more significant biases and scatter over high concentration regions. This bias in modeled NO$_2$ columns shown here is better than biases of more than 50 % in previous studies that used the GEOS-Chem model (e.g., Martin et al., 2006; Lin et al., 2010). The improvement of model performance here can be partly attributed to the more accurate power plant NO$_x$ emissions: the underestimation of modeled columns increased to 29 % in a sensitivity run with power plant emissions from the INTEX-B inventory (Zhang et al., 2009a) instead of the unit-based inventory. The finer model resolution may also play an important role.

Figure 6 shows the OMI and GEOS-Chem tropospheric NO$_2$ columns for the summers of 2005 and 2007 over China and their differences. Both model and OMI maps illustrate
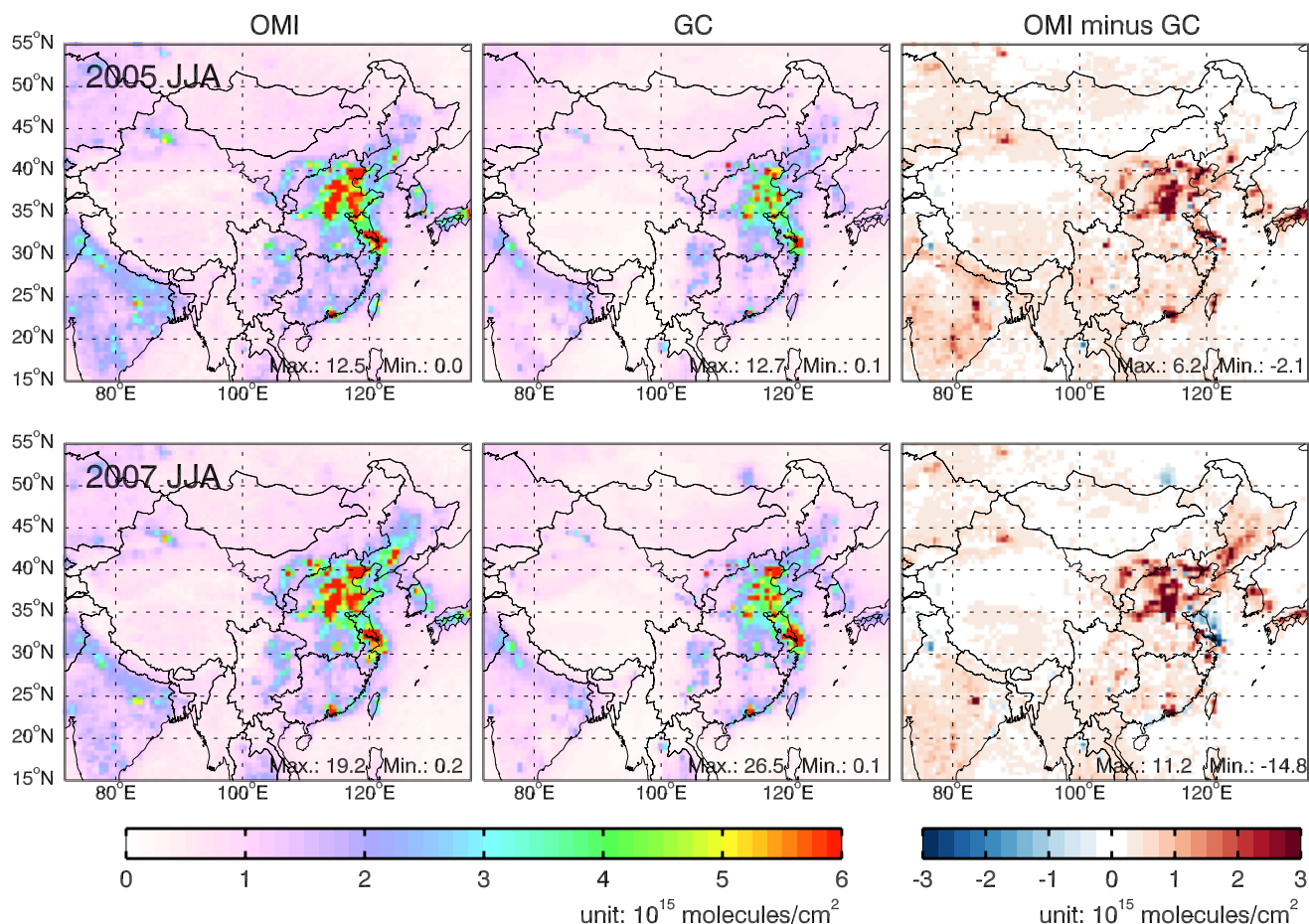
Fig. 6. OMI and GEOS-Chem tropospheric NO$_2$ columns for summers (JJA) of 2005 (top) and 2007 (bottom) and their differences.

that NO$_x$ emissions are concentrated in areas with dense energy consuming sources in eastern of China. Isolated metropolitan areas in northeastern and southeastern parts of China can be identified easily by OMI. Some individual large power plants located in rural areas are also obvious. However, the modeled NO$_2$ columns are significantly lower than OMI measurements by a factor of 2–3 in Shanxi-Shaanxi-Inner Mongolia region, where there are large coal reserves and many power plants and energy-consuming industrial complexes were built during the past decade. As power plant emissions can be well constrained by OMI, this difference possibly points to missing NO$_x$ emissions from other energy-intensive industries, which are widespread in these regions but are not well represented in the current bottom-up emission inventory and need to be further investigated (Zhang et al., 2009b). Another possible source of bias could come from errors in simulating NO$_x$ chemistry (Valin et al., 2011).

5 Increases of power plant NO$_x$ emissions in 2005–2007

5.1 Satellite observations of NO$_x$ emissions from new power plants

Figure 7a, b show the ratios of annual and summer average tropospheric NO$_2$ columns between 2007 and 2005 from OMI, respectively. The two small maps below each ratio map present the sample amounts used in the averages for the corresponding years. The new power plants are indicated as open circles in Fig. 7 (only the units coming into operation between June 2005 and August 2007 are plotted in Fig. 7b), with three symbol sizes from small to large indicating the total capacities of new generator units (<500 MW, 500–1200 MW, >1200 MW) in the corresponding power plants. The ratios are unreliable in background regions due to noise in satellite observations so that only those grids with average NO$_2$ columns $> 1.0 \times 10^{15}$ molecules cm^{-2} in both years are colored in the ratio maps.

Most of the distinct increases of NO$_2$ columns viewed by OMI during the two years are found to be collocated with
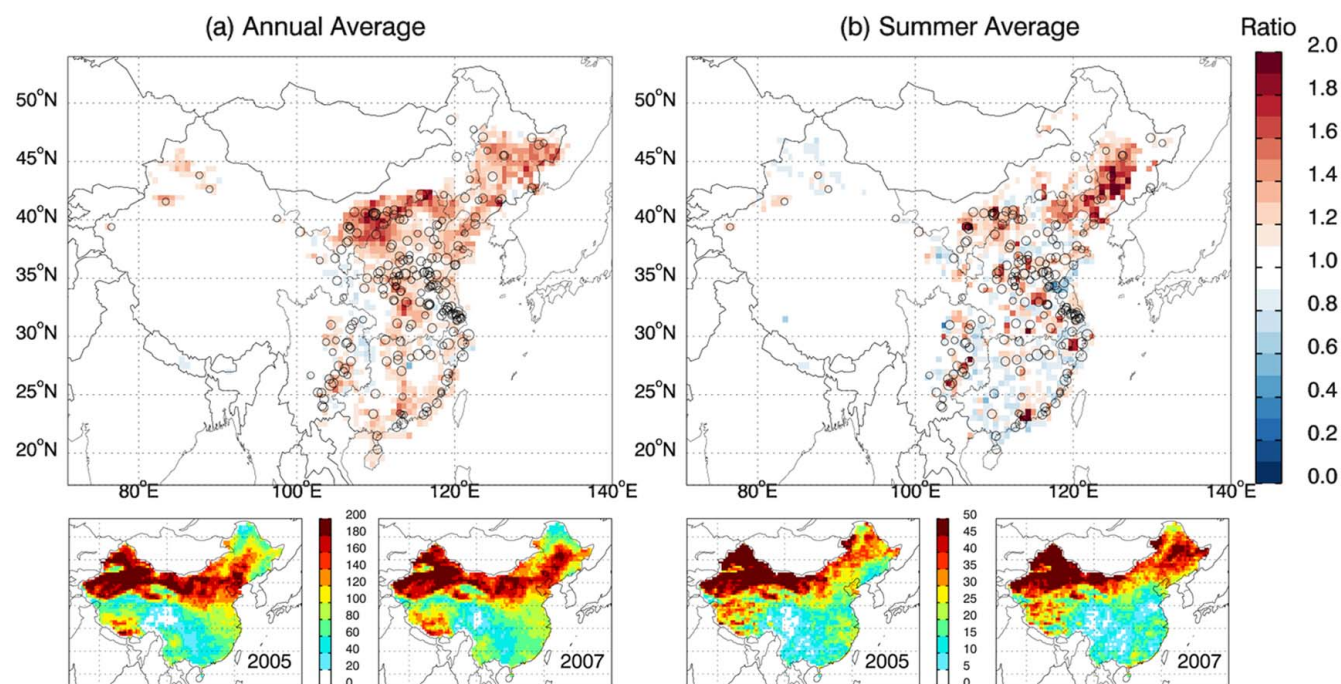
Fig. 7. Ratios of average OMI tropospheric NO$_2$ columns between 2007 and 2005 using **(a)** annual averages and **(b)** summer averages. Only grids inside Chinese boundary and with average NO$_2$ columns $>1.0 \times 10^{15}$ molecules cm^{-2} in both years are colored. Open circles denote the new power plants coming into operation during 2005–2007 (only new power plants coming into operation during June 2005–August 2007 are plotted in **(b)**), with three sizes from small to large: <500 MW, 500–1200 MW, >1200 MW. Small maps below each ratio map present the sample amounts used in the averages for the corresponding years (note change of scale).
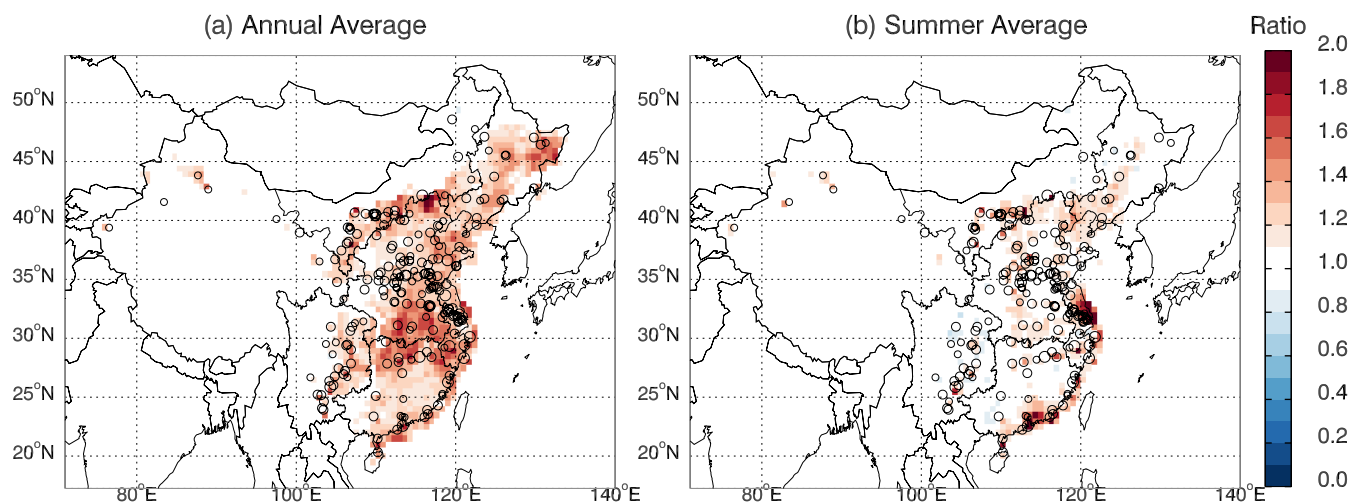
Fig. 8. Ratios of GEOS-Chem modeled tropospheric NO$_2$ columns between 2007 and 2005 using **(a)** annual averages and **(b)** summer averages. The cartography is same as Fig. 7.

the construction of new power plants in Fig. 7. North China and Inner Mongolia, as the main coal-manufacturing bases in China, contain a large number of new power plants and show the fastest growth rates of NO$_2$ columns in the entire country. East China and Southwest China also show large increases of NO$_2$ columns. In contrast, however, there are only a few new power plants in inland areas of South China and the NO$_2$ columns have not significantly increased in this region. It is noteworthy that there are significant increases in some grids without new power plants, and this could also be the result of atmospheric transport of NO$_x$. This is especially clear in the annual ratio map.
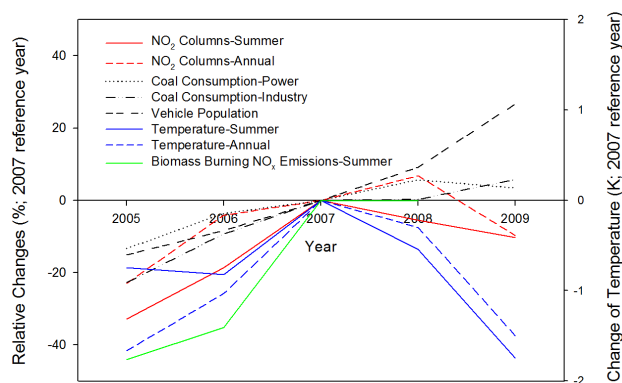
Fig. 9. Relative changes of annual and summer average OMI NO$_2$ columns, summertime biomass burning NO$_x$ emissions, and major annual anthropogenic activities, and absolute changes of annual and summer average temperature (2007 as reference year) during 2005–2009 in Northeast China. Summertime biomass burning emissions were taken from the GFED database (van der Werf et al., 2006).

Figure 8 presents the ratios of annual and summer average tropospheric NO$_2$ columns between 2007 and 2005 from the GEOS-Chem model. The modeled annual and summer ratios show similar spatial distributions as indicated by OMI, with the most significant increases in North China and Inner Mongolia and no significant increase in inland areas of South China. The growth rates of summer average columns in North China from OMI are higher than those from the model and have broader spatial extent, possibly related to some missing newly added industrial sources.

Many new power plant clusters locate in East China, but the ratios of NO$_2$ columns in this region are not as notable as those in North China and Inner Mongolia. This is due to the fact that East China has the most intensive NO$_x$ emissions in the whole country, and consequently, the observations of power plant emissions could be interfered with by the large contributions of emissions from other source types. There is a chain of new power plants in Sichuan, Chongqing, and Guizhou in Southwest China, visible in both the OMI and model data. But as the sample amounts of OMI measurements are very small (see Fig. 7) in summer in this region, due to the typical rainy weather, the ratios of summer average columns are not as distinct as the ratios of annual average columns in some grids.

The model shows significant increases of summer NO$_2$ columns over the new power plants in coastal regions of South China, while OMI observed decrease trend in summer columns over those locations. The reasons of this discrepancy remain unclear, but it is possible due to the undersampled a priori parameters in a large grid in NO$_2$ retrievals (Heckel et al., 2011), or inaccurate representation of coastal metrological filed in GESO-5 model. In Northeast China, OMI viewed significant increases of summer average NO$_2$ columns during 2005–2007, surpassing the variations of all

major anthropogenic indexes (shown in Fig. 9). Natural emissions may contribute to this increase because summer temperature and biomass burning activities in 2007 were the highest among 2005–2009 in Northeast China. However, further investigation is needed to confirm this guess.

In Fig. 10, we present five power plants as examples to show how OMI can identify the temporal evolution of NO$_x$ emissions over individual power plants with large new generator units. The NO$_2$ columns observed by OMI varied synchronously with the modeled columns, both surging dramatically (decreasing in Fig. 10e) after the new generator units came into operation. The successful identification of the emission evolutions over individual power plants using OMI measurements could be very useful for Ministry of Environmental Protection in China to monitor the current emission status and operations of pollutant control devices in power plants. However, this method greatly depends on the sample amounts and the location of power plants. Averaging and smoothing satellite observations for multi-years could provide more accurate top-down estimates on large point source emissions (Beirle et al., 2011; Fioletov et al., 2011), and we will extend the analysis for a longer period in our future work.

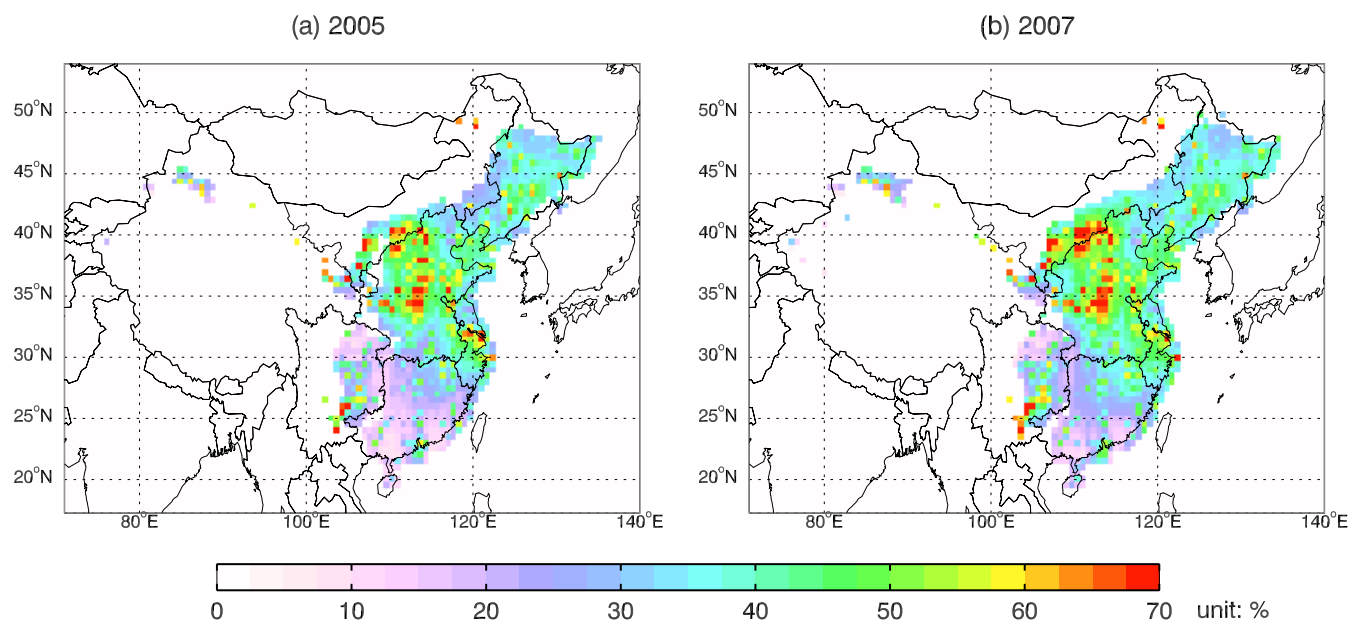## 5.2 Contributions of power plant emissions to NO$_2$ columns

In order to quantify the contributions of power plant NO$_x$ emissions to NO$_2$ columns, three scenarios with different power plant NO$_x$ emissions were examined in the nested-grid GEOS-Chem for the period of 2005–2007: (1), with the complete unit-based power plant emission inventory (hereinafter referred to simply as GC_PP); (2), without power plant emissions (hereinafter called GC_NoPP); and (3), with the unit-based power plant emission inventory for the same period, but without emissions from the generator units that came into operation in 2005–2007 (hereinafter called GC_NoNPP).

Figure 11 shows the relative contributions of the power plants to the annual average NO$_2$ columns in 2005 and 2007, which are defined as the relative differences between GC_PP and GC_NoPP. In Inner Mongolia, central North China and part of Southwest China, power plants contribute to more than 60 % of NO$_2$ columns. The share of power plant pollution was increased in Inner Mongolia and Southwest China during 2005–2007, where power plants dominated the increases of NO$_x$ emissions over that period. The share of power plant pollution decreased in mega-cities (e.g., Beijing and Guangzhou) as no new power plant was built in mega-cities and emissions from industries and transportation grew fast.

Figure 12 plots the relative contributions of the new power plants to the annual and summer average NO$_2$ columns in 2007, which are defined as the ratio of the difference between annual (or summer) average NO$_2$ columns in 2007
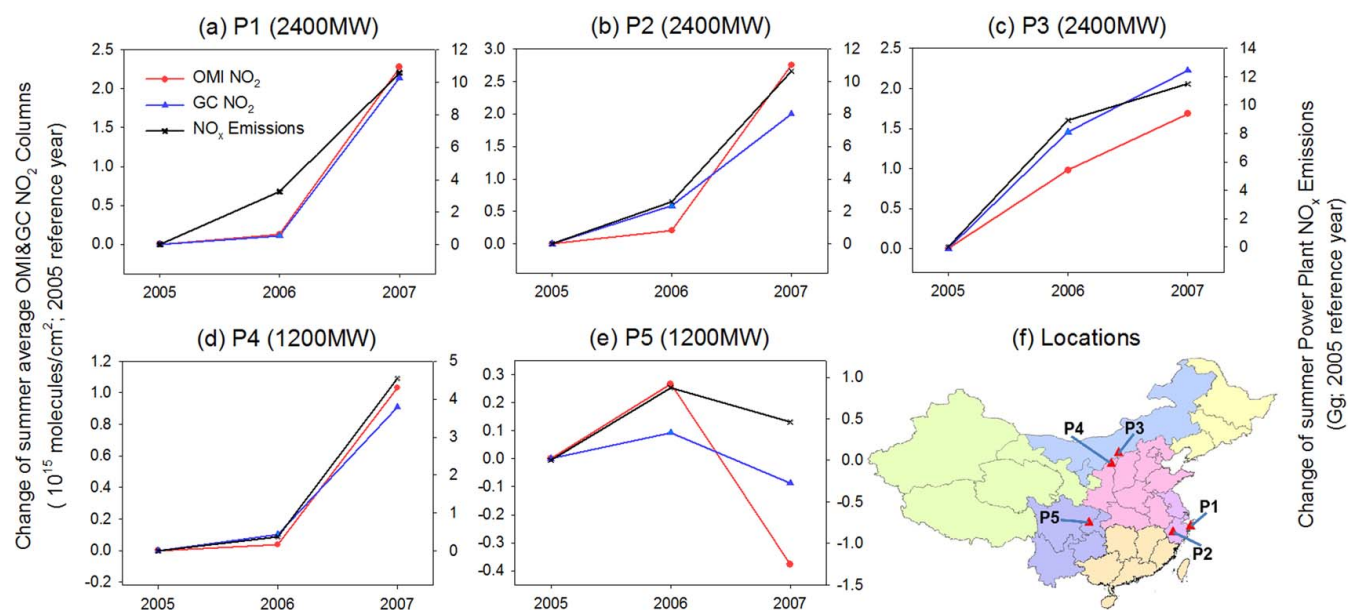
Fig. 10. Changes of summer average OMI and GEOS-Chem tropospheric NO$_2$ columns and power plant NO$_x$ emissions during 2005–2007 (2005 reference year) over five large new power plants. Numbers in the parentheses in the subtitles denote the new generation capacities added during June 2005–August 2007. Locations of the power plants are indicated in **(f)**.
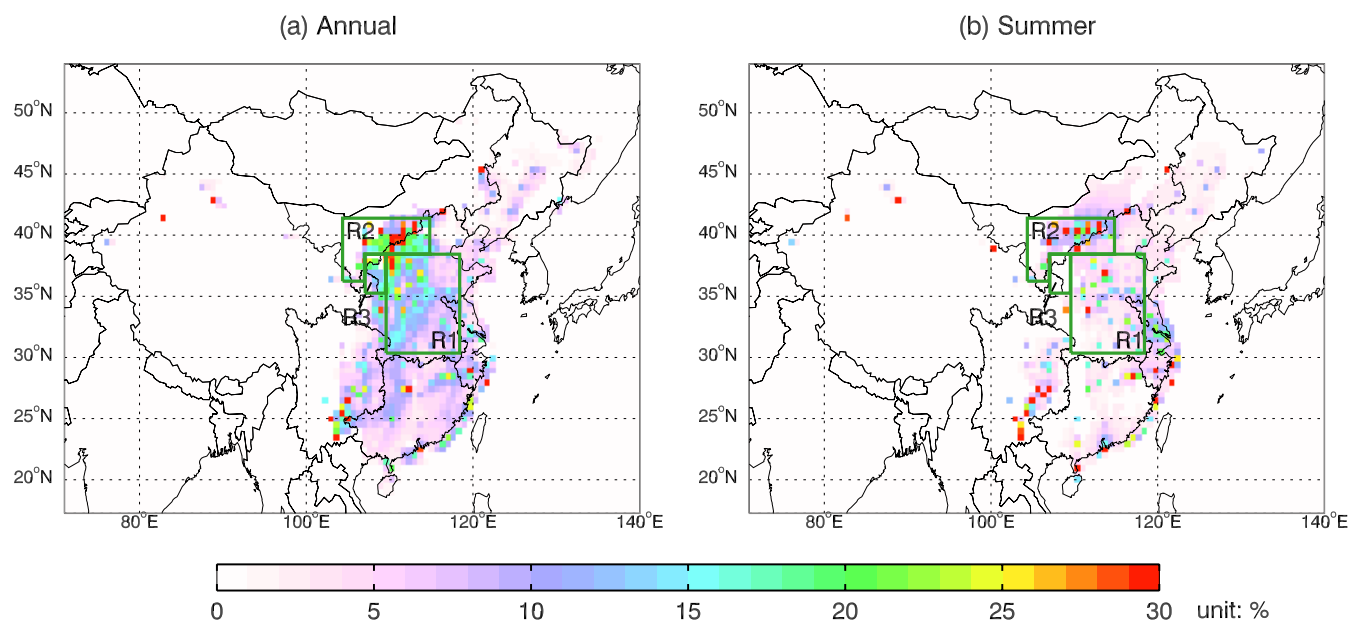

Fig. 11. Relative contributions of the power plant NO$_x$ emissions to the annual average NO$_2$ columns in **(a)** 2005 and **(b)** 2007, defined as the relative differences between GC_PP and GC_NoPP. Only grids inside Chinese boundary and with average NO$_2$ columns $>1.0 \times 10^{15}$ molecules cm^{-2} in GC_PP are colored.

from GC_PP and GC_NoNPP to the columns from GC_PP in 2007:

$$(\text{GC\_PP}_{2007} - \text{GC\_NoNPP}_{2007})/\text{GC\_PP}_{2007} \qquad (2)$$

As shown in Fig. 12, the impact of the new power plants are well constrained around the emitters in summer due to the short lifetime of NO$_x$, but expand over a wider scale in the annual average map as longer NO$_x$ lifetime in other seasons will allow NO$_x$ plumes from power plants transport to further distances. This is also consistent with the

Fig. 12. Relative contributions of the new power plant NO_x emissions to the **(a)** annual average NO_2 columns and **(b)** summer average NO_2 columns in 2007, defined as Eq. (2). Only grids inside Chinese boundary and with average NO_2 columns $>1.0 \times 10^{15}$ molecules cm^{-2} in GC_PP are colored. Domains of three studied regions are indicated in green rectangles.
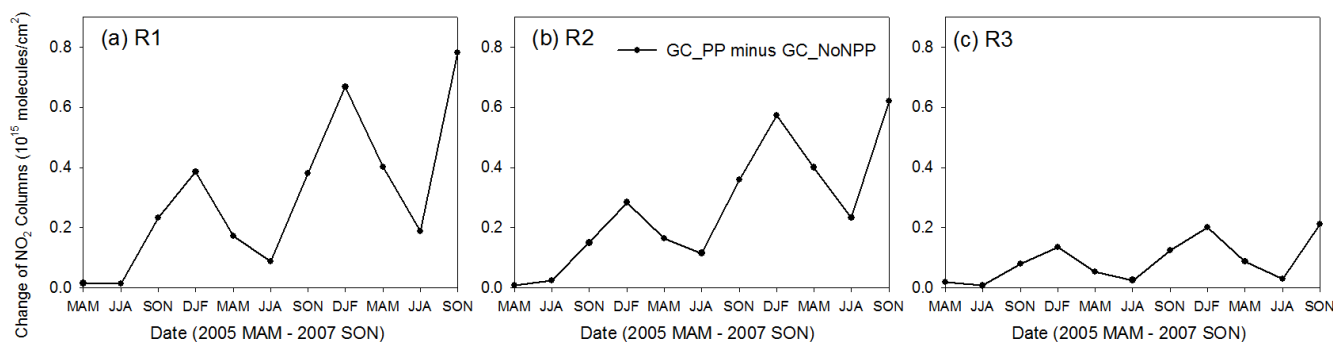
Fig. 13. Seasonal evolution of NO_2 columns from the new power plants, defined as the absolute differences between GC_PP and GC_NoNPP, during 2005 MAM to 2007 SON in the three regions in Fig. 12.

satellite observations presented in Fig. 7. In Fig. 12, R1 and R2 are two major regions with dramatic increases of NO_2 columns due to the new power plant emissions, as mentioned in Sect. 5.1; R3 is a background region where there is scarcely any anthropogenic source. New power plants contributed 10 % and 18.5 % to 2007 annual average NO_2 columns in R1 and R2, respectively, indicating the large environmental impact of new power plant constructions. New power plants have higher contribution to NO_2 columns in R2 compared to in R1 because power plant emissions in R2 are more dominant.

We further examined the evolution of NO_2 columns from the new power plants by season in three selected regions, as shown in Fig. 13. In R1 and R2, the increase of NO_2 columns due to new power plants shows a clear upward trend

with strong seasonal variations, reflecting the gradually increased contribution from new power plants and differences of NO_x lifetime in four seasons. The contributions of new power plants to NO_2 columns in R3 are very limited in summer, but could be up to 0.21×10^{15} molecules cm^{-2} in winter through transportation.

6 Impacts of new power plant NO_x emissions on satellite retrievals

The OMI tropospheric NO_2 column retrievals are sensitive to the changes in the a priori NO_2 shape factors used in the calculation of AMF. A new large surface emitter such as a power plant would cause a considerable change in the local NO_2
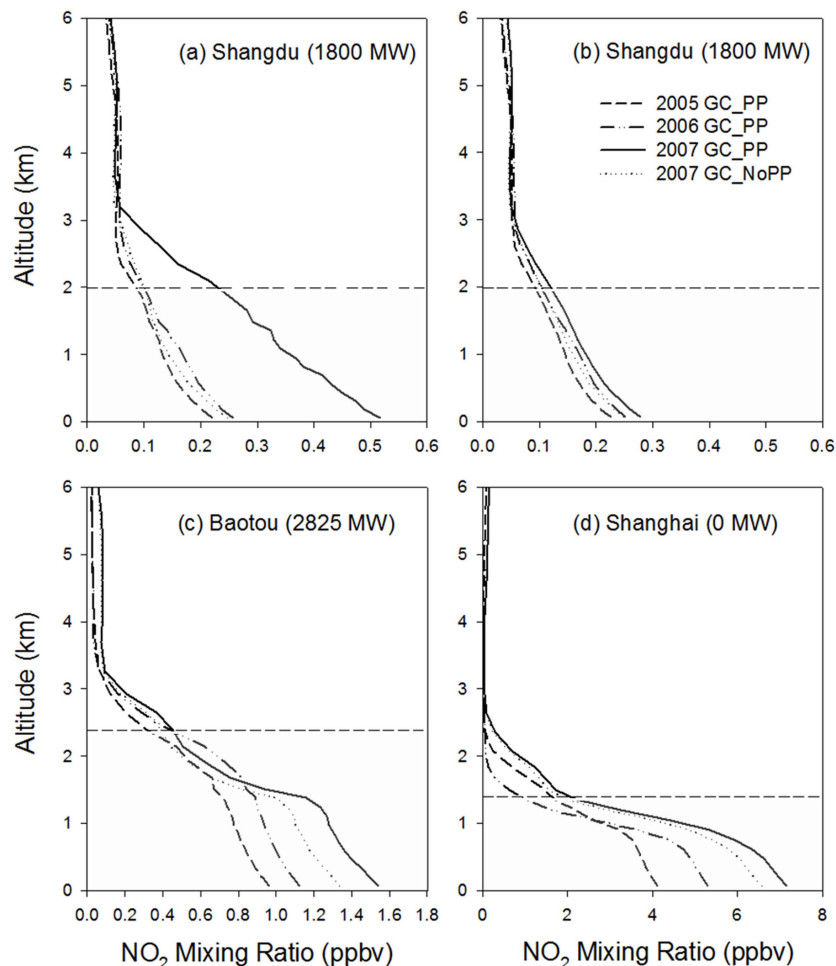
Fig. 14. NO$_2$ profiles from surface to 6 km for July in 2005–2007 generated from the nested-grid ($0.5° \times 0.667°$) GEOS-Chem model over Shangdu **(a)**, Baotou **(c)**, and Shanghai **(d)**, and from the $2° \times 2.5°$ GEOS-Chem model over Shangdu **(b)**. GC_PP denotes the GEOS-Chem simulations with all unit-based power plant emissions, and GC_NoNPP denotes the GEOS-Chem simulations without new power plant emissions. Dash lines indicate the average PBL heights. Numbers in the parentheses in the subtitles denote the new generation capacities added during June 2005–August 2007.

Table 4. Summer average OMI NO$_2$ columns derived with different a priori NO$_2$ profiles over various sites[a].

Site	Location	Category	New Capacity[b] (MW)	NO$_2$ Columns with $0.5° \times 0.667°$ profiles (10^{15} molecules cm^{-2})			NO$_2$ Columns with $2° \times 2.5°$ profiles (10^{15} molecules cm^{-2})	
				2005 GC_PP	2007 GC_PP	2007 GC_NoNPP	2005 GC_PP	2007 GC_PP
Shangdu	42.3° N,116.0° E	Rural	1800	1.25	2.00 (1.60)	1.79 (1.44)	1.15	1.66 (1.45)
Lingwu	38.1° N,106.5° E	Rural	1260	2.00	2.21 (1.11)	2.01 (1.01)	1.63	1.81 (1.11)
Lanxi	29.2° N,119.5° E	Town	2400	2.69	5.44 (2.02)	4.64 (1.72)	2.68	4.89 (1.82)
Tuoketuo	40.3° N,111.3° E	Town	2400	4.70	6.38 (1.36)	6.03 (1.28)	3.75	5.09 (1.36)
Baotou	40.7° N,109.7° E	Urban	2825	5.14	8.39 (1.63)	7.96 (1.55)	3.63	5.69 (1.57)
Wuhai	39.5° N,106.2° E	Urban	860	4.03	8.30 (2.06)	8.00 (1.99)	2.80	5.46 (1.95)
Shanghai	31.2° N,121.5° E	Metropolis	0	12.48	11.64 (0.93)	11.54 (0.92)	10.78	9.76 (0.91)
Beijing	39.9° N,116.4° E	Metropolis	0	7.50	10.52(1.40)	10.53 (1.40)	6.49	9.05'(1.39)

[a] Values in the parenthesis indicate the ratios of NO$_2$ columns in 2007 to the corresponding NO$_2$ columns in 2005.
[b] Capacities of new generator units which came into operation in June 2005–August 2007.

shape factor. However, this potential impact has not been explicitly considered yet in the operational space-borne products, because NO$_2$ shape factors are usually generated by a CTM driven by fixed emissions for all years.

We choose three representative cases to demonstrate the impacts of the new power plant NO$_x$ emissions on NO$_2$ profiles in Fig. 14: new power plants in rural area (Shangdu), new power plants in urban area (Baotou), and no new power plant in urban area (Shanghai). July-average NO$_2$ profiles from the nested-grid GEOS-Chem model for these three sites are presented in Fig. 14a, c, d, three from GC_PP for 2005–2007 and one from GC_NoNPP for 2007. To understand the impacts of new power plant emissions on NO$_2$ profiles at a coarser resolution, which are typically used in the operational satellite products, we conducted the 2° × 2.5° GEOS-Chem simulations for 2005–2007 with the same emission inputs used in the nested-grid GEOS-Chem model. Four July-average NO$_2$ profiles from the 2° × 2.5° GEOS-Chem model for Shangdu are presented in Fig. 14b. In Fig. 14a, the NO$_2$ concentrations in the lower atmosphere in Shangdu dramatically increased in 2007 due to the new power plant emissions added at the end of 2006. The differences between NO$_2$ profiles at 0.5° × 0.667° resolution from GC_PP and GC_NoNPP for 2007 are very significant up to 3 km in altitude, far above the PBL. In contrast, only minimal increases of NO$_2$ are found between the two profiles for 2007 in Fig. 14b, indicating that the impacts of new power plants on NO$_2$ profiles at the 2° × 2.5° resolution are not significant. In Baotou, an industrial city in Inner Mongolia, the surface NO$_2$ concentrations increased gradually in 2005–2007 along with the continuously added NO$_x$ emissions from both power plants and other anthropogenic sources. In Shanghai, the differences between NO$_2$ profiles from GC_PP and GC_NoNPP for 2007 are very small, while increases of NO$_x$ from other anthropogenic emissions contribute significantly to the changes of NO$_2$ profiles during 2005–2007.

Since the satellite is less sensitive to NO$_2$ in the lower atmosphere, the increase of surface NO$_2$ concentrations decreases the local AMF, and thus the retrieved tropospheric NO$_2$ columns would be underestimated in the grids with new power plants if no correction were conducted to the NO$_2$ shape factors. We compare summer average OMI NO$_2$ columns derived with different a priori NO$_2$ profiles over eight sites in Table 4. The NO$_2$ columns in summer 2007 calculated using GC_PP NO$_2$ profiles are 3.8–17.2 % higher than those calculated using GC_NoNPP NO$_2$ profiles over sites with new power plants, more significantly in rural areas and small towns. The simulation data at the nested-grid resolution (0.5° × 0.667°) used in this study could also improve the expression of the effects of new power plant emissions on the NO$_2$ profiles. The sensitivity analysis compared to OMI retrievals with NO$_2$ profiles generated from the global GEOS-Chem simulation (2° × 2.5°) suggests that the use of NO$_2$ profiles at 0.5° × 0.667° resolution could produce more significant growth rates over grids with new power plants

(see Table 4). In sites isolated from the populous regions, e.g., Shangdu and Lanxi, the effects from the resolution of the a priori NO$_2$ profiles used in the NO$_2$ retrievals can be up to 20 %, which obviously cannot be ignored in any trend analysis or quantification study.

It should be noted that the sensitivity analysis discussed here is subject to uncertainty. The fresh power plant plumes would not be laterally mixed within a 0.5° × 0.667° grid. Vertical distribution of emissions could vary within one model grid as functions of wind speed and downstream distances (Weil et al., 2004). Chemical transport model with finer horizontal resolutions and observation measurements should be used in future studies to reduce this uncertainty. Other parameters such as the aerosol profiles could also be affected by the new power plant emissions (SO$_2$ and NO$_x$) and cause some biases in the satellite retrievals. The scattering sulfate aerosols could increase the satellite's sensitivity to the NO$_2$ mixing in and above the aerosol layers (Leitão et al., 2010). However, there is no explicit correction for aerosol changes in the OMI product used in this work.

7   Concluding remarks

In this paper, we have demonstrated the rapid growth of power plant NO$_x$ emissions in 2005–2007 and their contributions to the increasing NO$_2$ columns in China, based on a unit-based power plant NO$_x$ emission inventory for mainland China, nested-grid GEOS-Chem model, and OMI observations. This inventory was based on a Chinese power plant database, and was validated through comparing the GEOS-Chem modeled NO$_2$ columns with OMI measurements in summers 2005 and 2007 over grids dominated by power plant NO$_x$ emissions. The major conclusions and implications can be drawn as follows.

The annual NO$_x$ emissions from coal-fired power plants were estimated to be 8.11 Tg, for 2005 and 9.58 Tg for 2007, respectively. The rapid growth of the power plant NO$_x$ emissions was mainly due to the 161.4 GW of new generator units constructed in the period of 2005–2007, which led to a 48.8 % increase of the coal-fired power generation capacity during this period. Generator units with size ≥300 MW accounted for 92.2 % of the total capacity additions. It is worth emphasizing that the structural readjustment in the power sector aimed at energy conservation and emission reduction is still in rapid progress and will have positive effects on the NO$_x$ emissions in China in the future.

The unit-based power plant NO$_x$ emissions were validated using the improved OMI NO$_2$ retrievals and the nested-grid GEOS-Chem model. The OMI-derived and GEOS-Chem-modeled summer average tropospheric NO$_2$ columns for 2005 and 2007 were well correlated ($R^2 = 0.79$–0.82) over grids dominated by power plant NO$_x$ emissions, with 7–14 % low bias in modeled NO$_2$ columns. This bias was within the uncertainty range of the power plant emission

estimates, lending support to the high accuracy of the unit-based power plant NO$_x$ emission inventory. The comparisons involving more grids produced more scatter over grids with elevated NO$_2$ concentrations, indicating that NO$_x$ emissions were relatively poorly understood over the regions where power plant emissions were mixed with other anthropogenic sources. This validated power plant inventory also facilitates forward investigations of the emissions in other anthropogenic sources by separating the power plant emissions out.

OMI observed dramatic increases of NO$_2$ columns during 2005–2007 in China attributed to the construction of new power plants. North China and Inner Mongolia showed the fastest growth rates of NO$_2$ columns in the country, followed by East China. Infrequent sampling in the Sichuan Basin and South China made it difficult to capture the signals of some new power plants in summer. The coarse-resolution a priori NO$_2$ shape factors used in the satellite retrievals also reduced the accuracy of NO$_2$ columns near the coastline, introducing an additional bias in the observations of new power plants there. We found that OMI had the capability to trace the changes of NO$_x$ emissions over individual power plants, e.g., the addition of new generator units, in the cases where there was less interference from other NO$_x$ sources. This application can be used to provide useful information to the environmental officials to monitor the emissions and evaluate the possible reductions due to the application of control devices in power plants in the future.

Sensitivity analysis with two scenarios of GEOS-Chem simulations, with and without new power plant emissions, suggested that the relative contributions of these new power plants to the annual average NO$_2$ columns in 2007 were 10 % in North China and 18.5 % in Inner Mongolia. The contribution of new power plants to NO$_2$ columns in North China showed a clear upward trend with strong seasonal variations, reflecting the gradually increased contribution from new power plants and differences of NO$_x$ lifetime in four seasons.

The new power plant NO$_x$ emissions can have a significant impact on the satellite retrieval by changing the NO$_2$ shape factor. The effects from new power plant emissions caused 3.8–17.2 % increases in the summer average OMI tropospheric NO$_2$ columns for the six selected sites, more significantly in rural areas and small towns. The fine-resolution data used in this study improved the expression of the effects of new power plant emissions on the NO$_2$ profiles, especially in areas isolated from the populous regions, resulted in up to 20 % increases of the summer average NO$_2$ column ratios between 2007 and 2005 compared to OMI retrievals with NO$_2$ profiles generated from a global GEOS-Chem simulation ($2° \times 2.5°$). It is worth considering the use of a priori shape factors generated by a CTM with temporally varying bottom-up emissions and at a reasonably high resolution in the operational satellite retrieval products. The changes of aerosols and plume chemistry over the new power plants should also be further investigated in the future.

Edited by: I. Aben

References

Baughcum, S. L., Tritz, T. G., Henderson, S. C., and Pickett, D. C.: Scheduled civil aircraft emission inventories for 1992: database development and analysis, NASA CR-4700, NASA, Washington DC, USA, 1996.

Beirle, S., Boersma, K. F., Platt, U., Lawrence, M. G., and Wagner, T.: Megacity emissions and lifetimes of nitrogen oxides probed from space, Science, 333, 1737–1739, 2011.

Bey, I., Jacob, D. J., Yantosca, R. M., Logan, J. A., Field, B. D., Fiore, A. M., Li, Q. B., Liu, H. Y., Mickley, L. J., and Schultz, M. G.: Global modeling of tropospheric chemistry with assimilated meteorology: Model description and evaluation, J. Geophys. Res., 106, 23073–23095, doi:10.1029/2001JD000807, 2001.

Bhaduri, B., Bright, E., Coleman, P., and Dobson, J.: LandScan: locating people is what matters, Geoinfomatics, 5, 34–37, 2002.

Boersma, K. F., Bucsela, E., Brinksma, E., and Gleason, J. F.: NO$_2$, in: OMI Algorithm Theoretical Basis Document, vol. IV, Trace Gas Algorithms, edited by: Chance, K., NASA Goddard Space Flight Cent., Greenbelt, Md, 15–36, 2002.

Boersma, K. F., Eskes, H. J., and Brinksma, E. J.: Error analysis for tropospheric NO$_2$ retrieval from space, J. Geophys. Res., 109, D04311, doi:10.1029/2003JD003962, 2004.

Boersma, K. F., Eskes, H. J., Veefkind, J. P., Brinksma, E. J., van der A, R. J., Sneep, M., van den Oord, G. H. J., Levelt, P. F., Stammes, P., Gleason, J. F., and Bucsela, E. J.: Near-real time retrieval of tropospheric NO$_2$ from OMI, Atmos. Chem. Phys., 7, 2103–2118, doi:10.5194/acp-7-2103-2007, 2007.

Boersma, K. F., Eskes, H. J., Dirksen, R. J., van der A, R. J., Veefkind, J. P., Stammes, P., Huijnen, V., Kleipool, Q. L., Sneep, M., Claas, J., Leitão, J., Richter, A., Zhou, Y., and Brunner, D.: An improved tropospheric NO$_2$ column retrieval algorithm for the Ozone Monitoring Instrument, Atmos. Meas. Tech., 4, 1905–1928, doi:10.5194/amt-4-1905-2011, 2011.

Bovensmann, H., Burrows, J. P., Buchwitz, M., Frerick, J., Noël, S., Rozanov, V. V., Chance, K. V., and Goede, A. P. H.: SCIA-MACHY: Mission objectives and measurement modes, J. Atmos. Sci., 56, 127–150, 1999.

Bucsela, E. J., Celarier, E. A., Wenig, M. O., Gleason, J. F., Veefkind, J. P., Boersma, K. F., and Brinksma, E. J.: Algorithm for NO$_2$ vertical column retrieval from the Ozone Monitoring

Instrument, IEEE T. Geosci. Remote Sens., 44, 1245–1258, doi:10.1109/TGRS.2005.863715, 2006.

Carn, S. A., Krueger, A. J., Krotkov, N. A., Yang, K., and Levelt, P. F.: Sulfur dioxide emissions from Peruvian copper smelters detected by the Ozone Monitoring Instrument, Geophys. Res. Lett., 34, L09801, doi:10.1029/2006GL029020, 2007.

Celarier, E. A., Brinksma, E. J., Gleason, J. F., Veefkind, J. P., Cede, A., Herman, J. R., Ionov, D., Goutail, F., Pommereau, J.-P., Lambert, J.-C., van Roozendael, M., Pinardi, G., Wittrock, F., Schönhardt, A., Richter, A., Ibrahim, O. W., Wagner, T., Bojkov, B., Mount, G., Spinei, E., Chen, C. M., Pongetti, T. J., Sander, S. P., Bucsela, E. J., Wenig, M. O., Swart, D. P. J., Volten, H., Kroon, M., and Levelt, P. F.: Validation of ozone monitoring instrument nitrogen dioxide columns, J. Geophys. Res., 113, D15S15, doi:10.1029/2007JD008908, 2008.

Chen, D., Wang, Y., McElroy, M. B., He, K., Yantosca, R. M., and Le Sager, P.: Regional CO pollution and export in China simulated by the high-resolution nested-grid GEOS-Chem model, Atmos. Chem. Phys., 9, 3825–3839, doi:10.5194/acp-9-3825-2009, 2009.

Clarke, M. R. B.: The reduced major axis of a bivariate sample, Biometrika, 67, 441–446, doi:10.1093/biomet/67.2.441, 1980.

Dirksen, R. J., Boersma, K. F., Eskes, H. J., Ionov, D. V., Bucsela, E. J., Levelt, P. F., and Kelder, H. M.: Evaluation of stratospheric NO$_2$ retrieved from the Ozone Monitoring Instrument: intercomparison, diurnal cycle and trending, J. Geophys. Res., 116, D08305, doi:10.1029/2010JD014943, 2011.

Eskes, H. J. and Boersma, K. F.: Averaging kernels for DOAS total-column satellite retrievals, Atmos. Chem. Phys., 3, 1285–1291, doi:10.5194/acp-3-1285-2003, 2003.

Fioletov, V. E., McLinden, C. A., Krotkov, N., Moran, M. D., and Yang, K.: Estimation of SO$_2$ emissions using OMI retrievals, Geophys. Res. Lett., 38, L21811, doi:10.1029/2011GL049402, 2011.

Ghude, S. D., Fadnavis, S., Beig, G., Polade, S. D., and van der A, R. J.: Detection of surface emission hot spots, trends, and seasonal cycle from satellite-retrieved NO$_2$ over India, J. Geophys. Res., 113, D20305, doi:10.1029/2007JD009615, 2008.

Hains, J. C., Boersma, K. F., Kroon, M., Dirksen, R. J., Cohen, R. C., Perring, A. E., Bucsela, E., Volten, H., Swart, D. P. J., Richter, A., Wittrock, F., Schoenhardt, A., Wagner, T., Ibrahim, O. W., van Roozendael, M., Pinardi, G., Gleason, J. F., Veefkind, J. P., and Levelt, P.: Testing and improving OMI DOMINO tropospheric NO$_2$ using observations from the DANDELIONS and INTEX-B validation campaigns, J. Geophys. Res., 115, D05301, doi:10.1029/2009JD012399, 2010.

Hao, J. M., Tian, H. Z., and Lu, Y. Q.: Emission inventories of NO$_x$ from commercial energy consumption in China, 1995–1998, Environ. Sci. Technol., 36, 552–560, 2002.

Heckel, A., Kim, S.-W., Frost, G. J., Richter, A., Trainer, M., and Burrows, J. P.: Influence of low spatial resolution a priori data on tropospheric NO$_2$ satellite retrievals, Atmos. Meas. Tech., 4, 1805–1820, doi:10.5194/amt-4-1805-2011, 2011.

Jaeglé, L., Steinberger, L., Martin, R. V., and Chance, K.: Global partitioning of NO$_x$ sources using satellite observations: Relative roles of fossil fuel combustion, biomass burning and soil emissions, Faraday Discus., 130, 407–423, doi:10.1039/b502128f, 2005.

Kim, S.-W., Heckel, A., McKeen, S. A., Frost, G. J., Hsie, E.-Y., Trainer, M. K., Richter, A., Burrows, J. P., Peckham, S. E., and Grell, G. A.: Satellite-observed U.S. power plant NO$_x$ emission reductions and their impact on air quality, Geophys. Res. Lett., 33, L22812, doi:10.1029/2006GL027749, 2006.

Kim, S.-W., Heckel, A., Frost, G. J., Richter, A., Gleason, J., Burrows, J. P., McKeen, S., Hsie, E.-Y., Granier, C., and Trainer, M.: NO$_2$ columns in the western United States observed from space and simulated by a regional chemistry model and their implications for NO$_x$ emissions, J. Geophys. Res., 114, D11301, doi:10.1029/2008JD011343, 2009.

Konovalov, I. B., Beekmann, M., Richter, A., and Burrows, J. P.: Inverse modelling of the spatial distribution of NO$_x$ emissions on a continental scale using satellite data, Atmos. Chem. Phys., 6, 1747–1770, doi:10.5194/acp-6-1747-2006, 2006.

Lamsal, L. N., Martin, R. V., van Donkelaar, A., Celarier, E. A., Bucsela, E. J., Boersma, K. F., Dirksen, R., Luo, C., and Wang, Y.: Indirect validation of tropospheric nitrogen dioxide retrieved from the OMI satellite instrument: Insight into the seasonal variation of nitrogen oxides at northern midlatitudes, J. Geophys. Res., 115, D05302, doi:10.1029/2009JD013351, 2010.

Lamsal, L. N., Martin, R. V., Padmanabhan, A., van Donkelaar, A., Zhang, Q., Sioris, C. E., Chance, K., Kurosu, T. P., and Newchurch, M. J.: Application of satellite observations for timely updates to global anthropogenic NO$_x$ emission inventories, Geophys. Res. Lett., 38, L05810, doi:10.1029/2010GL046476, 2011.

Leitão, J., Richter, A., Vrekoussis, M., Kokhanovsky, A., Zhang, Q. J., Beekmann, M., and Burrows, J. P.: On the improvement of NO$_2$ satellite retrievals – aerosol impact on the airmass factors, Atmos. Meas. Tech., 3, 475–493, doi:10.5194/amt-3-475-2010, 2010.

Levelt, P. F., van den Oord, G. H. J., Dobber, M. R., Mälkki, A., Visser, H., de Vries, J., Stammes, P., Lundell, J. O. V., and Saari, H.: The Ozone Monitoring Instrument, IEEE T. Geosci. Remote Sens., 44, 1093–1101, doi:10.1109/TGRS.2006.872333, 2006.

Li, C., Zhang, Q., Krotkov, N. A., Streets, D. G., He, K. B., Tsay, S.-C., and Gleason, J. F.: Recent large reduction in sulfur dioxide emissions from Chinese power plants observed by the Ozone Monitoring Instrument, Geophys. Res. Lett., 37, L08807, doi:10.1029/2010GL042594, 2010.

Lin, J.-T.: Satellite constraint for emissions of nitrogen oxides from anthropogenic, lightning and soil sources over East China on a high-resolution grid, Atmos. Chem. Phys., 12, 2881–2898, doi:10.5194/acp-12-2881-2012, 2012.

Lin, J.-T. and McElroy, M. B.: Detection from space of a reduction in anthropogenic emissions of nitrogen oxides during the Chinese economic downturn, Atmos. Chem. Phys., 11, 8171–8188, doi:10.5194/acp-11-8171-2011, 2011.

Lin, J. T., McElroy, M. B., and Boersma, K. F.: Constraint of anthropogenic NO$_x$ emissions in China from different sectors: a new methodology using multiple satellite retrievals, Atmos. Chem. Phys., 10, 63–78, doi:10.5194/acp-10-63-2010, 2010.

Martin, R. V., Jacob, D. J., Chance, K., Kurosu, T. P., Palmer, P. I., and Evans, M. J.: Global inventory of nitrogen oxide emissions constrained by space-based observations of NO$_2$ columns, J. Geophys. Res., 108, 4537, doi:10.1029/2003JD003453, 2003.

Martin, R. V., Sioris, C. E., Chance, K., Ryerson, T. B., Bertram, T.
H., Wooldridge, P. J., Cohen, R. C., Andy Neuman, J., Swanson,
A., and Flocke, F. M.: Evaluation of space-based constraints on
global nitrogen oxide emissions with regional aircraft measure-
ments over and downwind of eastern North America, J. Geophys.
Res., 111, D15308, doi:10.1029/2005JD006680, 2006.

Ohara, T., Akimoto, H., Kurokawa, J., Horii, N., Yamaji, K., Yan,
X., and Hayasaka, T.: An Asian emission inventory of an-
thropogenic emission sources for the period 1980–2020, At-
mos. Chem. Phys., 7, 4419–4444, doi:10.5194/acp-7-4419-2007,
2007.

Olivier, J. G. J. and Berdowski, J. J. M.: Global emissions sources
and sinks, in: The Climate System, Lisse, The Netherlands, 33–
78, 2001.

Palmer, P. I., Jacob, D. J., Chance, K., Martin, R. V., Spurr, R. J.
D., Kurosu, T. P., Bey, I., Yantosca, R., Fiore, A., and Li, Q.
B.: Air mass factor formulation for spectroscopic measurements
from satellites: Application to formaldehyde retrievals from the
Global Ozone Monitoring Experiment, J. Geophys. Res., 106,
14539–14550, doi:10.1029/2000JD900772, 2001.

Platt, U.: Differential Optical Absorption Spectroscopy (DOAS), in:
Air Monitoring by Spectroscopic Techniques, John Wiley, New
York, USA, 27–84, 1994.

Richter, A., Burrows, J. P., Nüß, H., Granier, C., and Niemeier, U.:
Increase in tropospheric nitrogen dioxide over China observed
from space, Nature, 437, 129–132, 2005.

Sauvage, B., Martin, R. V., van Donkelaar, A., and Ziemke, J. R.:
Quantification of the factors controlling tropical tropospheric
ozone and the South Atlantic maximum, J. Geophys. Res., 112,
D11309, doi:10.1029/2006JD008008, 2007.

Schaub, D., Brunner, D., Boersma, K. F., Keller, J., Folini, D., Buch-
mann, B., Berresheim, H., and Staehelin, J.: SCIAMACHY tro-
pospheric NO$_2$ over Switzerland: estimates of NO$_x$ lifetimes and
impact of the complex Alpine topography on the retrieval, At-
mos. Chem. Phys., 7, 5971–5987, doi:10.5194/acp-7-5971-2007,
2007.

Schneider, A., Friedl, M. A., and Potere, D.: A new map of global
urban extent from MODIS satellite data, Environ. Res. Lett., 4,
044003, doi:10.1088/1748-9326/4/4/044003, 2009.

Streets, D. G., Bond, T. C., Carmichael, G. R., Fernandes, S. D., Fu,
Q., He, D., Klimont, Z., Nelson, S. M., Tsai, N. Y., Wang, M.
Q., Woo, J.-H., and Yarber, K. F.: An inventory of gaseous and
primary aerosol emissions in Asia in the year 2000, J. Geophys.
Res., 108, 8809, doi:10.1029/2002JD003093, 2003.

Tian, H.: Studies on Present and Future Emissions of Nitrogen Ox-
ides and Its Comprehensive Control Policies in China, Ph. D.
thesis, Tsinghua Univ., Beijing, 2003.

Valin, L. C., Russell, A. R., Hudman, R. C., and Cohen, R.
C.: Effects of model resolution on the interpretation of satel-
lite NO$_2$ observations, Atmos. Chem. Phys., 11, 11647–11655,
doi:10.5194/acp-11-11647-2011, 2011.

van der A, R. J., Eskes, H. J., Boersma, K. F., van Noije, T. P. C.,
Van Roozendael, M., De Smedt, I., Peters, D. H. M. U., and Mei-
jer, E. W.: Trends, seasonal variability and dominant NO$_x$ source
derived from a ten year record of NO$_2$ measured from space, J.
Geophys. Res., 113, D04302, doi:10.1029/2007JD009021, 2008.

van der Werf, G. R., Randerson, J. T., Giglio, L., Collatz, G. J.,
Kasibhatla, P. S., and Arellano Jr., A. F.: Interannual variabil-
ity in global biomass burning emissions from 1997 to 2004, At-
mos. Chem. Phys., 6, 3423–3441, doi:10.5194/acp-6-3423-2006,
2006.

van Donkelaar, A., Martin, R. V., Leaitch, W. R., Macdonald, A. M.,
Walker, T. W., Streets, D. G., Zhang, Q., Dunlea, E. J., Jimenez,
J. L., Dibb, J. E., Huey, L. G., Weber, R., and Andreae, M. O.:
Analysis of aircraft and satellite measurements from the Inter-
continental Chemical Transport Experiment (INTEX-B) to quan-
tify long-range transport of East Asian sulfur to Canada, At-
mos. Chem. Phys., 8, 2999–3014, doi:10.5194/acp-8-2999-2008,
2008.

Wang, S. W., Streets, D. G., Zhang, Q., He, K. B., Chen, D.,
Kang, S. C., Lu, Z. F., and Wang, Y. X.: Satellite detection and
model verification of NO$_x$ emissions from power plants in North-
ern China, Environ. Res. Lett., 5, 044007, doi:10.1088/1748-
9326/5/4/044007, 2010.

Wang, Y., Jacob, D. J., and Logan, J. A.: Global simulation of tropo-
spheric O$_3$-NO$_x$-hydrocarbon chemistry, 1. Model formulation,
J. Geophys. Res., 103(D9), 10713–10726, 1998.

Wang, Y. X., McElroy, M. B., Martin, R. V., Streets, D. G., Zhang,
Q., and Fu, T.-M.: Seasonal variability of NO$_x$ emissions over
east China constrained by satellite observations: Implications
for combustion and microbial sources, J. Geophys. Res., 112,
D06301, doi:10.1029/2006JD007538, 2007.

Weil, J. C., Sullivan, P. P., and Moeng, C.-H.: The use of large-eddy
simulations in Lagrangian particle dispersion models, J. Atmos.
Sci., 61, 2877–2887, 2004.

Wenig, M., Spichtinger, N., Stohl, A., Held, G., Beirle, S., Wagner,
T., Jähne, B., and Platt, U: Intercontinental transport of nitro-
gen oxide pollution plumes, Atmos. Chem. Phys., 3, 387–393,
doi:10.5194/acp-3-387-2003, 2003.

Yevich, R. and Logan, J. A.: An assessment of biofuel use and burn-
ing of agricultural waste in the developing world, Global Bio-
geochem. Cy., 17, 1095, doi:10.1029/2002GB001952, 2003.

Yienger, J. J. and Levy, U. H.: Empirical model of global soil-
biogenic NO$_x$ emissions, J. Geophys. Res., 100, 11447–11464,
1995.

Zhang, Q., Streets, D. G., He, K. B., Wang, Y. X., Richter, A., Bur-
rows, J. P., Uno, I., Jang, C. J., Chen, D., Yao, Z. L., and Lei, Y.:
NO$_x$ emission trends for China, 1995–2004: The view from the
ground and the view from space, J. Geophys. Res., 112, D22306,
doi:10.1029/2007JD008684, 2007.

Zhang, Q., Streets, D. G., Carmichael, G. R., He, K. B., Huo, H.,
Kannari, A., Klimont, Z., Park, I. S., Reddy, S., Fu, J. S., Chen,
D., Duan, L., Lei, Y., Wang, L. T., and Yao, Z. L.: Asian emis-
sions in 2006 for the NASA INTEX-B mission, Atmos. Chem.
Phys., 9, 5131–5153, doi:10.5194/acp-9-5131-2009, 2009a.

Zhang, Q., Streets, D. G., and He, K. B.: Satellite observations
of recent power plant construction in Inner Mongolia, China,
Geophys. Res. Lett., 36, L15809, doi:10.1029/2009GL038984,
2009b.

Zhao, C. and Wang, Y. H.: Assimilated inversion of NO$_x$ emissions
over east Asia using OMI NO$_2$ column measurements, Geophys.
Res. Lett., 36, L06805, doi:10.1029/2008GL037123, 2009.

Zhao, Y., Wang, S. X., Duan, L., Lei, Y., Cao, P. F., and Hao, J. M.: Primary air pollutant emissions of coal-fired power plants in China: Current status and future prediction, Atmos. Environ., 42, 8442–8452, 2008.

Zhao, Y., Nielsen, C. P., Lei, Y., McElroy, M. B., and Hao, J: Quantifying the uncertainties of a bottom-up emission inventory of anthropogenic atmospheric pollutants in China, Atmos. Chem. Phys., 11, 2295–2308, doi:10.5194/acp-11-2295-2011, 2011.